Contributions to Geophysics and Geodesy Vol. 55/3, 2025 (313–339)

Synthetic 2D GPR constant-offset radargrams: Modelling of responses of air-filled cavities with various shapes

Farhad HAMEKHANI, Roman PAŠTEKA*

Department of Engineering geology, Hydrogeology and Applied Geophysics,
Faculty of Sciences, Comenius University, Ilkovičova 6, 842 15 Bratislava, Slovak Republic

Abstract: The present study describes results from synthetic modelling of 2D GPR constant-offset radargrams (B-scans) for air-filled cavities with different shapes. The primary objective of these simulations was to enhance the understanding of actual GPR data when subsurface cavities are present. Three different numerical methods are used, based on the Finite-Difference Time Domain approach. During processing of received synthetic radargrams, migration plays a crucial role. When designing the final depth-sections, it proved to be extremely important the application of the so-called Combined Time–Depth Conversion transformation method. Final results showed with good precision the geometry and depth extent of studied cavities in the absolute majority of the calculated models. The verified processing steps sequence was also successfully applied to a real-world dataset from GPR survey data from St. Catherine's church in Banská Štiavnica.

Key words: archaeogeophysics, GPR, modelling, crypts, cavity detection

1. Introduction

Ground penetrating radar (GPR, or in simple terms "georadar") is one of the most important methods in near-surface geophysics. The GPR method has found applications in many areas: ranging from solving engineering, environmental, hydrogeological, geotechnical, forensic, glaciological problems – to non-destructive archaeological research (e.g., *Daniels, 2004; Annan, 2003; Reynolds, 2011*). The GPR technique in archaeology is one of the standard non-destructive prospecting methods (*Basile et al., 2000; Leckebusch, 2000; Lorenzo et al., 2002; Linford, 2006; Leucci and De Giorgi, 2010; Haynes et al., 2023; Cuenca-Garcia et al., 2024* and many others). The detection of naturally occurring and artificial cavities is one of the important objectives of GPR surveys, as cavities are usually objects with a significant contrast in electric petrophysical properties to their soil (rock)

*corresponding author, e-mail: roman.pasteka@uniba.sk

doi: 10.31577/congeo.2025.55.3.3

surroundings (e.g., *Morey, 1974* in *Smith and Jol, 1995; Kuhns 1983; Martinaud et al., 2004; Daniels, 2004; Annan, 2003; Reynolds, 2011; Persico et al., 2014; Solla et al., 2016; Persico et al., 2019; Panisova et al., 2016; Leucci et al., 2021; Persico et al., 2024*).

Several authors have published studies describing the basic characteristics of anomalous wave images in GPR data in the case of cavity detection. Based on practical experience, it can be stated that cavities are mainly characterized by a pronounced reflection (with high amplitudes) from their upper edge and a possible reflection from the bottom edge (*Persico et al., 2024*). Besides this, typical is the presence of reverberations due to probable multiple reflections and occurrence of so-called "X-shaped features" (will be explained later) in the un-migrated B-scans (*ibid.*). Some other authors (*Martinaud et al., 2004*) point to the fact that right angles between vertical walls and floor in the bottom of the cavity can produce additional disturbing signals – so-called dihedral corner signals (will be explained later).

The present study focuses on anomalous features in 2D radargrams (B-scans) in the case of shallow cavities, occurring in historical buildings and complexes: crypts, tombs, cellars, corridors, etc. This type of cavity is relatively easy to detect by means of the GPR method, but their anomalous patterns can be sometimes very complex (influenced by diffraction waves and multiples). In our opinion, from the 2D radargrams it is only possible to determine the depth and shape of the upper edge with certainty. Determining the depth and shape of the lower edge is more difficult. Using synthetic modelling, we attempted to visualize different types of cavities, mainly with different shapes in their cross-section. We show that, through an accurate numerical modelling and by careful analysis of processed 2D radargrams, valuable information about their geometry can be obtained.

In general, several methods have been proposed to numerically simulate GPR data. These techniques include ray-based methods (*Goodman, 1994; Cai and McMechan, 1995*), frequency-domain methods (*Prokopidis and Tsiboukis, 2007; Zeng et al., 1995*) and pseudospectral methods (*Carcione, 1996; Casper and Kung, 1996; Liu and Fan, 1999*). But, of all these listed methods, the Finite-Difference Time Domain (FDTD) approach seems to be the most widely used, and it has been developed over the last few decades as a standard method for modelling GPR wave propagation (e.g., *Wang and Tripp, 1996; Bourgeois and Smith, 1996; Bergmann et al., 1996; Teixeira*

et al., 1998; Giannopoulos, 2005; Irving and Knight, 2006). In this paper, we have chosen three software solutions, which are based on the FDTD approach: a) the simplified solution (so-called "Exploding-Reflector") in the commercial software ReflexW (*Sandmeier, 2020*); b) the algorithm from *Irving and Knight (2006)*, together with their MATLAB script and finally c) the well-known algorithm GPRmax (*Giannopoulos, 2005*). There exist differences among the concepts and numerical schemes in these three used methods – and for this reason, after initial independent testing, we decided to use all of them in the this paper.

Synthetic radargrams contain the basic information about the modelled cavity, but they must be further processed – with the aim to "strip" the fundamental information about the depth, size and geometry of the studied cavity. During the processing of modelled synthetic GPR data, we have applied several important calculation steps, like migration and removal of multiples (with ReflexW software and in-house MATLAB script). We have also used the so-called Combined Time–Depth Conversion (CTDC) transformation from *Persico et al. (2024)*, to improve the calculation of final depth sections. This approach is working with a velocity model of the section, which uses different values for the surrounding soil (rock) and for the interior of the interpreted cavity. This is very helpful, especially for the estimation of the depth of the cavity lower edge. We show that an appropriate use of a GPR survey data, supported by well-selected processing steps, allows not only the detection of the subsurface cavity but also the retrieval of detailed information on its shape, in particular returning its upper edge curvature. Such results are critical for enhancing the interpretability and applicability of GPR in complex subsurface settings.

The main objective of the article is to better understand the manifestations of modelled cavities in the reflection field (which has a slight educational dimension) and to find a processing procedure that can extract as much information as possible from the data about the actual shape (and dimensions) of the detected cavities. We demonstrate the basic properties of anomalous patterns in the case of shallow cavities in several synthetic examples, which build the main part of this paper (additional examples are provided in the Supplementary Material). In addition to synthetic examples, we also offer an example of real data processing: GPR survey data from St. Catherine's church in Banská Štiavnica.

2. Methodology

We will start in this chapter with the explanation of the modelling procedures and describing the occuring features in the resulting radargrams. Then we will continue with the processing steps needed to improve the visibility of cavities in the synthetic radargrams.

The presented publication deals with numerical modelling of air-filled cavities that often occur in non-destructive archaeological (archaeo-geophysical) research – crypts, tombs, cellars, tunnels, etc. The strong contrast between two environments in the case of air-filled cavities (soil/air) is one of the most striking examples of the application of near-surface geophysical methods. Based on the above, the use of geoelectric/EM methods (mainly GPR) is often successful in detecting and defining of air-filled cavities. The basis for explaining the properties of EM waves in the GPR method in the case of reflection and refraction into air-filled cavities is the description of contrasts in EM petrophysical properties (electric permittivity, electric conductivity and magnetic permeability).

In this study, we use synthetic datasets generated by simulation of underground cavities models with the Finite-Difference Time Domain (FDTD) approach. The FDTD approach to the numerical solution of Maxwell's equations (first-order partial differential equations) is to discretize both the space and time continua (*Giannopoulos, 2005*). In the presented study, we have used three different software solutions of the FDTD approach:

a) The first software solution is the commercial software ReflexW (*Sandmeier, 2020*), a well-known and used processing tool in GPR practice. This software uses a simplified solution for the 2D direct problem of propagation of EM waves by means of the FDTD method, the so-called "Exploding-Reflector". We understand this concept as very close to the known Huygens-Fresnel principle in wave-physics, in which every point of boundaries acts as a source of secondary waves, propagating through media. This ReflexW solution does not calculate reflections from the top surface soil/air boundary, which makes the resulting synthetic radargrams more simple, but far away from real datasets. On the other hand, it can help better to understand phenomena, which occur in the cavity and its close surroundings. Another great advantage is that anomalous structures of variable forms can be modelled.

b) The second software solution is the MATLAB script from authors *Irving and Knight (2006)*, which involves also the FDTD method in two dimensions, using the transverse magnetic mode formulation. Computation time is higher, when comparing it with the ReflexW software, but on the other hand the Irving and Knight method calculates reflections from the top surface soil/air boundary, which makes the resulting synthetic radargrams closer to the real data-sets. Also here, anomalous structures of variable forms can be modelled.

c) The third software is the well-known algorithm GPRmax, which is widely used by the GPR expert community and is based on the paper from *Giannopoulos (2005)* and following publications (e.g. *Warren et al., 2016*). It uses the so-called Yee's algorithm to solve Maxwell's equations in 3D using the Finite-Difference Time-Domain (FDTD) method. The finite difference expressions for the spatial and temporal derivatives are central-difference in nature and second-order accurate (*GPRmax website, n.d.*). A great advantage is the 3D approach and possibility to use as sources of modelled EM waves simulations of real GPR antennas (e.g. GSSI). Disadvantages of this algorithm are: This method encounters two main problems because it needs longer computation time and it cannot accurately model complex shapes of cavities, since curved structures have to be approximated through staircases in the rectangular grid. This algorithm again calculates reflections from the top surface soil/air boundary.

Although, usually the field GPR data are collected in TE mode (transverse-electric), the numerical modelling was performed in TM mode (transverse-magnetic), which is a common approximation in GPR studies. This difference does not significantly affect the interpretation of our results. In the case of all three used software, we have used the frequency of the source equal to 100 MHz. This frequency is suitable for the detection of objects with dimensions, which are typical for the searched cavities in archaeo-geophysical researches (crypts, tombs, cellars, corridors, etc.).

During numerical modelling of GPR data, it is important to analyse the propagation velocities of EM waves in the obtained outputs. Velocity (speed) of EM waves in different materials and environments can be calculated by formulas, derived from the EM field theory. In the case of simplified

ideal dielectric materials with low loss (conductivity = 0, relative magnetic permeability = 1), a simplified formula is valid (*Reynolds, 2011, p. 539*):

$$v = c/\sqrt{\varepsilon_r} = 0.3/\sqrt{\varepsilon_r} \quad [\mathrm{m/ns}]\,. \tag{1}$$

In this contribution we work in all presented models with the contrast of two environments: soil and air. In the case of a dry soil (sand), we consider the typical value of the relative electric permittivity $\varepsilon_r = 9$ (this value fits into the interval 5 – 10 for coastal dry sands in Table 13.4 from *Reynolds 2011, p. 551*), which results in the velocity value $v = 0.1$ m/ns. In the case of air we have the well-known value $\varepsilon_r = 1$, which results into the velocity value $v = 0.3$ m/ns (typical value of EM waves in air).

When understanding the complex reflection pattern in the case of anomalous cavity manifestations in 2D radargarms (B-scans), it is also important to analyse the polarity of the recorded EM waves. The change of the polarity of reflected waves is given by the reflection coefficient (Γ), which is determined by the contrast in the intrinsic impedances of adjacent media (e.g. *Pozar, 2012, p. 29*). Again, in the simplified ideal dielectric case (electric conductivity = 0, relative magnetic permeability = 1) of two layers with dielectric constants $\varepsilon_{r,1}$ and $\varepsilon_{r,2}$, the generally used formula has the form:

$$\Gamma = \frac{\sqrt{1/\varepsilon_{r,2}} - \sqrt{1/\varepsilon_{r,1}}}{\sqrt{1/\varepsilon_{r,2}} + \sqrt{1/\varepsilon_{r,1}}}\,. \tag{2}$$

In the case when EM waves penetrate the boundary from soil ($\varepsilon_{r,1} = 9$) into air in the cavity ($\varepsilon_{r,2} = 1$), reflection coefficient (Eq. 2) has the value +0.5. In the opposite case, when EM waves are penetrating the boundary from the air into the soil, the calculated reflection coefficient (Eq. 2) has the value −0.5. The aforementioned change in polarity can be observed in several synthetic results in this paper, but it is sometimes difficult to observe this phenomenon in the practical datasets, because the reflections from bottom edges of cavities are often masked by resulting multiples in these situations. We can nicely demonstrate this change of wave amplitude polarity in the case of a simple prism with rectangular cross-section (Fig. 1a, width = 5 m, height = 3 m). Depth of the upper edge of the prism is 1 m, which gives for the velocity of soil ($v = 0.1$ m/ns) the value of the two-way time (TWT) = 20 ns (first important flat reflection in Fig. 1b). After the

EM waves enter into the cavity, the velocity increases to the velocity of EM waves in air ($v = 0.3$ m/ns): this fact will cause the occurrence of the next important flat reflection in the 2D radargram (Fig. 1b) for the TWT value of 40 ns (20 ns in the soil plus 20 ns in the air, the height of the cavity is 3 m). The polarity of this second important reflection from the bottom edge has reversed character (Fig. 1b), due to the negative reflection coefficient in the case air/soil. This can be seen also in the cases of rectangular prisms with different vertical dimensions (Supplementary Material, figures SM 1-1, SM 1-2, SM 1-3, SM 1-4, SM 1-5 and SM 1-6; left-hand column – solutions from the ReflexW software).

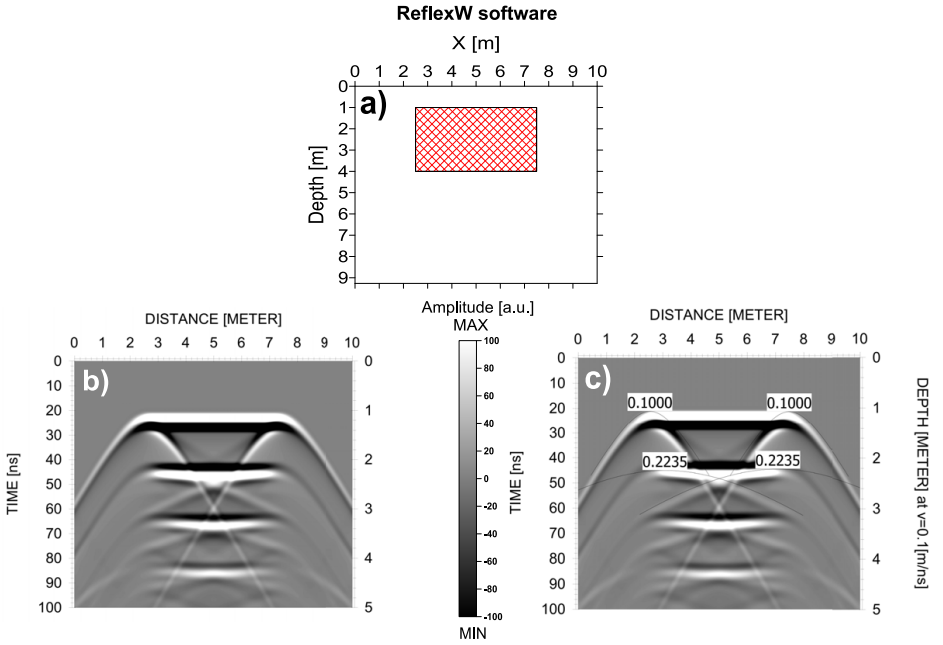

Fig. 1. Model of a cavity with rectangular cross-section (width = 5 m, height = 3 m). a) vertical depth-section of the model (surrounding soil: $\varepsilon_1 = 9$, air in the cavity: $\varepsilon_2 = 1$); b) original synthetic 2D radargram (ReflexW software); c) original synthetic 2D radargram (ReflexW) with marked important diffraction hyperbolas and estimated velocities.

Another very important aspect of the complex reflection pattern in the case of cavities is the occurrence of multiple reflections (multiples) for the higher TWT values in the 2D radargrams. There are occurring two main types of multiples in the case of shallow cavity models:

– The first type arises within the cavity itself and is dominant. It always occurs for larger TWT values than the first reflection of the bottom edge. As it can be seen in Fig. 1b, polarity of these multiples remains identical as it was in the case of the first reflection from the bottom edge of the cavity (because there occur two next reflections from the boundary air/soil, which will return the amplitudes polarity back to that from bottom edge). This phenomenon can be nicely seen in next examples of rectangular prisms with different vertical dimensions (Figs. 2 and 3; and

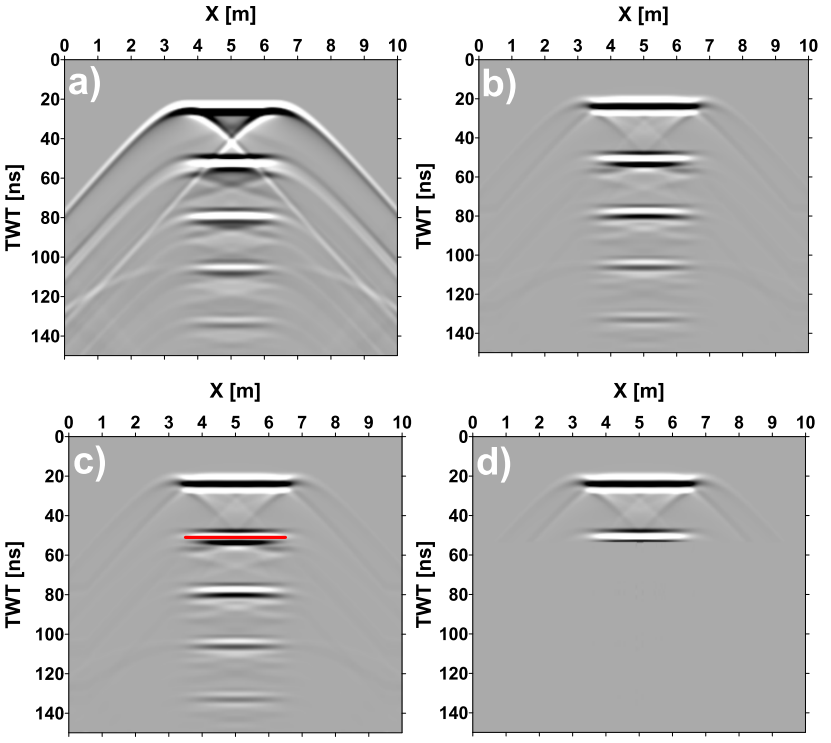

Fig. 2. Sequence of partial outputs from the GPR data 2D processing of synthetic model results in the form of vertical radargrams: a) synthetic radargram of an air-filled cavity model with rectangular cross-section (width = 3 m, height = 4 m), generated using the FD method in ReflexW software; b) migrated section using Kirchhoff migration with a combining window width of 100 traces; c) identification of internal multiple reflections for removal (short red line shows the reflection, which should remain in the final section as the deepest one); d) final radargram after multiple suppression (time range = 60 ns, time lag = 40 ns, number of multiples = 4, number of traces = 5).

Figs. SM 1-1, SM 1-2, SM 1-3, SM 1-4 and SM 1-5 in the Supplementary Material, for smaller vertical dimensions of the prisms also the TWT distances between the multiples become smaller).

– The second type of a multiple arises from repeated reflection of EM waves from the top surface (soil/air). This type of reflection occurs deeper than the first significant reflection of the upper edge (this often falls into the TWT interval of the cavity) and is usually less pronounced. Its TWT position can be easily calculated – it is located in integer multiples of the TWT value of the first significant reflection from the upper edge. It can be easily identified in the cases of cavities with high vertical dimension (Fig. 4 and Fig. 5), but it can be hardly recognised in the case of cavities with small vertical dimension (Supplementary Material, figures SM 1-4 and SM 1-5 – solutions from the GPRmax algorithm), where it interferes with the reflection from the bottom edge and multiples of the first type.

Together, both types of described multiples can sometimes create together a relatively complex interference pattern (Supplementary Material, figures SM 1-4 and SM 1-5 – solutions from the GPRmax algorithm), which in some cases can complicate the interpretation of the lower edge of the cavity. In the next part of the paper, we will show several examples of such

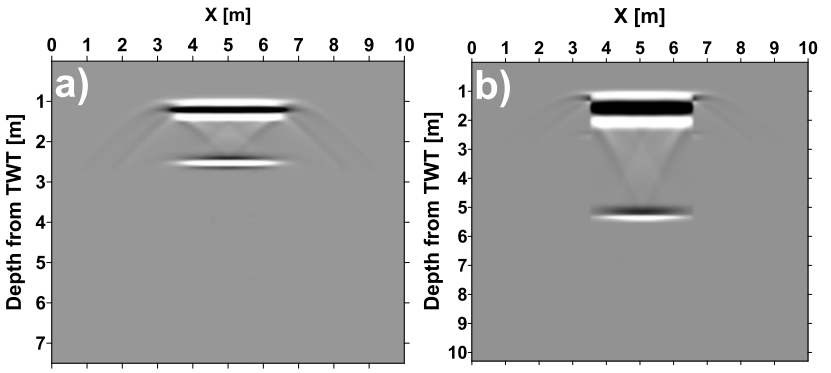

Fig. 3. Sequence of outputs showing time–depth conversion results for an air-filled cavity model with rectangular cross-section (width = 3 m, height = 4 m): a) depth estimate using a conventional single uniform velocity method (0.1 m/ns), showing an improper lower edge depth; b) correct depth estimate using the Combined Time–Depth Conversion (CTDC) transformation with two velocities: for soil (0.1 m/ns) and for air (0.3 m/ns inside the cavity).

situations for modelled cavities with different shapes (in cross-section) and horizontal/vertical dimensions. It is important to mention here that the synthetic data outputs from ReflexW software do not produce the multiples from the top surface boundary (soil/air), so received 2D radargrams from this software have more simple "character", in comparison with the outputs from *Irving and Knight (2006)* method and from the GPRmax software. On the other hand, solutions from the ReflexW help to understand the basic character of the anomalous wave pattern without the influence of the top surface boundary (soil/air).

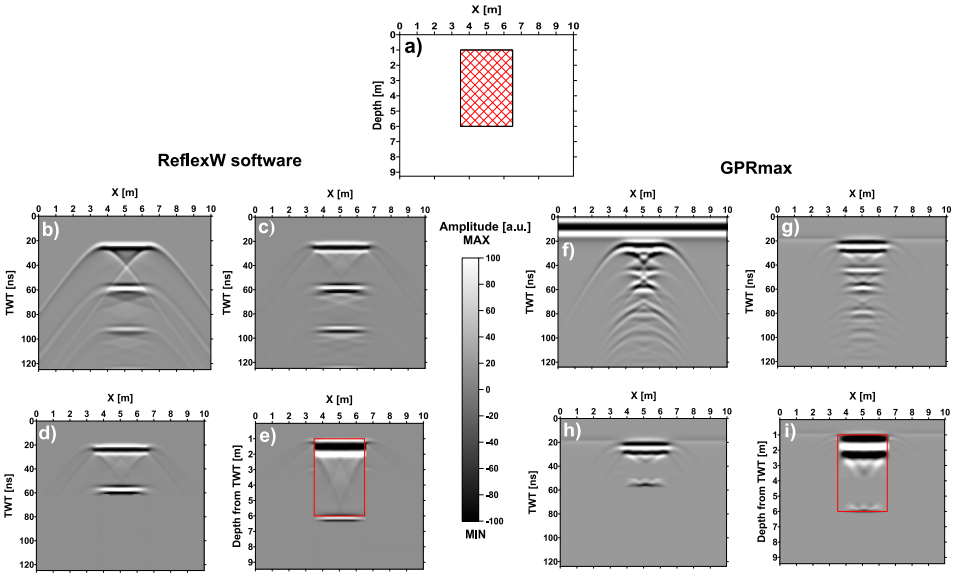

Fig. 4. Comparison of processed 2D synthetic radargrams of modelled cavity structure with rectangular cross-section (width = 3 m, height = 5 m). Panel a) shows the vertical depth-section of the model (with identical petrophysical parameters as in Fig. 1); Panels b) – e) show the results of the ReflexW software: b) the original synthetic radargram, c) migrated version, d) version with removed multiples and e) result from applied CTDC transformation with the outline of the original model (red). Panels f) – i) show the results of the GPRmax software for the same sequence of processing steps as in b) – e). In radargrams g) – i) additional background removal was applied. In radargrams h) – i) additional removal of the multiple from the top of the model was applied. Red contours in e) and i) show the cross-section of the cavity structure. Processing parameters used: summation width (applied during migration) = 75 for ReflexW results and 40 for GPRmax and method results, migration velocity = 0.1 m/ns.

In some situations, we can remove both types of the multiples from the radargram during processing of the modelled data. The first type of multiple can be well removed by means of the special tool of the ReflexW software (functionality "Multiple Reflection"), where the user has to specify four parameters: time range, time lag, number of multiples and number of traces. This kind of removal is influencing usually the bottom part of the radargram (for higher TWT values than the reflection from the bottom edge of the cavity), which is not so important for the interpretation. Example of such removal application will be shown in Fig. 2c and Fig. 2d; and it will be

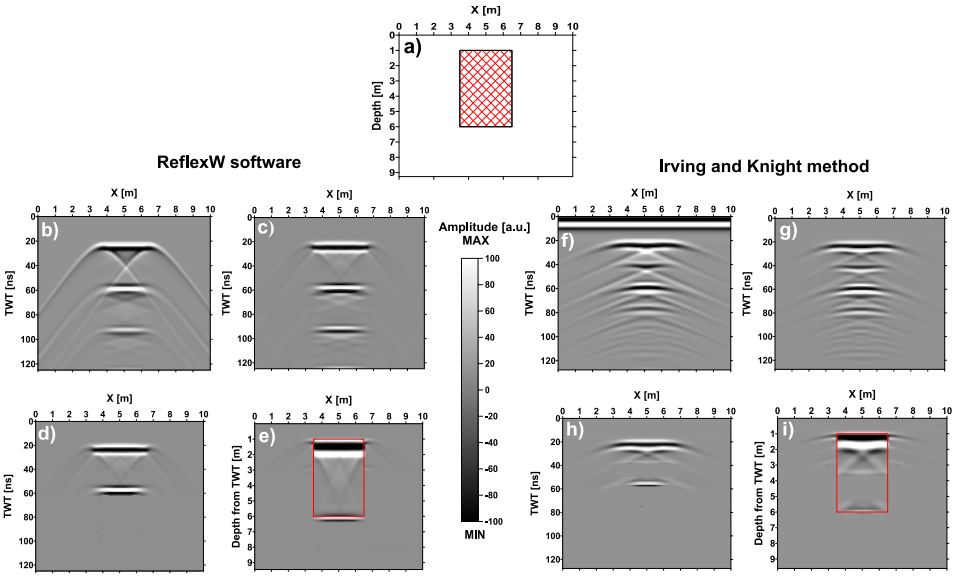

Fig. 5. Comparison of processed 2D synthetic radargrams of modelled cavity structure with rectangular cross-section (width = 3 m, height = 5 m). Panel a) shows the vertical depth-section of the model (with identical petrophysical parameters as in Fig. 1); Panels b) – e) show the results of the ReflexW software: b) the original synthetic radargram, c) migrated version, d) version with removed multiples and e) result from applied CTDC transformation with the outline of the original model (red). Panels f) – i) show the results of the Irving and Knight method for the same sequence of processing steps as in b) – e). In radargrams g) – i) additional background removal was applied. In radargrams h) – i) additional removal of the multiple from the top of the model was applied. Red contours in e) and i) show the cross-section of the cavity structure. Processing parameters used: summation width (applied during migration) = 75 for ReflexW results and 40 for GPRmax and Irving-Knight method results, migration velocity = 0.1 m/ns.

later applied during the processing of all synthetic examples and practical dataset. To remove the second type of multiple we have created a simple in-house MATLAB script, which is very similar to the numerical solution in ReflexW. It is based on the removal of amplitudes (in a defined window) that occur at integer multiples of the TWT value from the first important reflection (from the upper edge of the cavity). The user has to specify four parameters: TWT of the first important reflection, TWT interval (which will be then removed), begin of the window in x-direction and end of the window in x-direction. In the case of this second type of multiple we have often a more complicated situation (when comparing it with the first type of multiple), because this kind of multiple can occur also for smaller TWT values and can interfere with the reflection from the bottom edge. In such a case, the user has to decide if to remove this kind of multiple or not.

Besides the important reflections from the upper and bottom boundaries of the cavity, there occur diffraction waves at the terminations of these edges (corner points of the prism). Inside the expected interior of the cavity (prism), or in deeper parts of the radargram, "wings" (side parts) of these diffraction hyperbolas intersect in a typical pattern, which is resembling the letter "X". This so-called "X-shape" was pointed out in papers from several authors (*Utsi 2017* in *Persico et al., 2019; Persico et al., 2024*) and we can follow it in the majority of our synthetic results (starting with Fig. 1b and 1c). Very interesting is the occurrence of so-called dihedral (or corner) signals (*Martinaud et al., 2004*), which originates when an EM beam bounces twice on perpendicular flat reflectors (in bottom corners of the cavity). This is causing an existence of a specular reflection, which occurs very near to the main reflection from the bottom edge of the cavity. This phenomenon can be followed in many practical datasets, but is hardly to be modelled – because the majority of software solutions work with horizontal and sub-horizontal reflectors (not with vertical reflectors).

When analysing the velocities obtained from 2D radargrams in their deeper parts, it is necessary to take into account that EM waves pass through multiple layers and objects with different propagation velocities. In such cases, it is necessary to consider the average speed, and in practice, the so-called RMS (Root Mean Square) velocity v_{RMS}, which is the square root of the average squared velocity (*Yilmaz, 2001*):

$$v_{\mathrm{RMS}} = \sqrt{\sum_{i=1}^{N} v_i^2 \Delta t_i \Big/ \sum_{i=1}^{N} \Delta t_i}\,, \tag{3}$$

where v_i is the velocity in the i-th layer and Δt_i is the two-way time in the same layer. It is quite clear that in our case, this RMS velocity is only a rough approximation, as it was derived for a horizontally layered homogeneous medium. The results of fitting velocity hyperbolas to the results from some synthetic models indicate that the use of this approximation is justified. Using the example in Fig. 1 with velocities: $v_1 = 0.1$ m/ns, $v_2 = 0.3$ m/ns and TWT values: $\Delta t_1 = 20$ ns, $\Delta t_2 = 20$ ns, we receive the value for the RMS velocity (Eq. 3): $v_{\mathrm{RMS}} = 0.2236$ m/ns. This value fits with high precision with the estimated velocity from the deeper diffraction hyperbolas (starting from the bottom corners of the modelled cavity) in Fig. 1c and was also identified in the next model results (e.g. in Figs. SM4-1 and SM4-2, simulating pits with an air-filled layer above them; Supplementary Material document).

The original synthetic 2D radargrams obtained from modelling software (Fig. 1 and next examples) need to be further processed in order to be better interpreted – with the aim of determining the geometry of the cavity. Some processing steps can significantly clean up the given sections – mainly migration and removal of multiples. For this processing, we have used the ReflexW software and also in-house MATLAB scripts. In Fig. 2 we brought an example of such processing flow – in the case of a modelled cavity with rectangular cross-section (width = 3 m, height = 4 m). We can see that in the comparison with the original radargram (Fig. 2a), its migrated version (Fig. 2b) has suppressed diffraction waves from the corners of the cavity. Later we will show that besides this important improvement also the shapes of upper and bottom boundaries of the cavity will improve their form. In our calculations, we have used the known Kirchhoff migration – with a combining window of 100 traces. Next step was the removal of the multiples (the first type of the multiple). The ReflexW Processing software allows the user to define manually a selected reflection (Fig. 2c, red line-segment), which will be then automatically removed from the radargram. In Fig. 2d we display the result of this operation. It can be seen that in this result, two dominant planar reflections are defining the upper and bottom edge of the cavity. Final step in our processing sequence is the calculation of the depth

section. When we took the time-section in Fig. 2d and have used the constant velocity for soil (0.1 m/ns) for the time-to-depth recalculation, then we obtained a depth-section (Fig. 3a), in which the depth of the upper edge of the cavity is correct (1 m), but the depth of the bottom edge is incorrect (2.5 m). This is a well-known fact, caused by the different velocity of the EM waves in the air-filled cavity. When we have processed this step by means of the so-called Combined Time–Depth Conversion (CTDC) method from *Persico et al. (2024)* (using an in-house MATLAB script), then we have received a correct result (Fig. 3b), where the depth of the bottom edge of the cavity is in the right position – in the depth of 5 m. The CTDC method is based on the approach This method is based on an approach that uses a velocity model in which the correct air velocity is calculated within the expected cavity. Of course that by means of the creation of the velocity model we are shifted into the interpretation part, but in the case of cavities with rectangular cross-section, this can be done relatively easily – vertical dimension of the cavity can be estimated from the two-way times of the dominant reflection and also its horizontal dimension. This will not be so easy, when we will deal with cavities of irregular cross-sectional shapes (this will be shown later).

In the next part of the paper (chapter Results) we will bring results of synthetic modelling (for cavities with different shapes of cross-sections) and processing of the obtained results by means of the presented processing flow.

3. Results

Main features of the GPR constant-offset 2D radargrams in the case of a cavity with rectangular cross-section were introduced in the methodological part of this paper (Figs. 1, 2 and 3). Here we continue with further results of our numerical modelling – focusing on cavities with various shapes of cross-sections. In all presented examples (Figs. 4–11) we present the results from ReflexW software and the Irving and Knight method (in Fig. 4 the GPRmax method), where we have used the same work-flow of processing steps: migration, removal of multiples and finally the Combined Time–Depth Conversion (CTDC) transformation. We start with a rectangular cavity (but with different dimensions, as used before) and then we present

models of cavities with various shapes of the upper edge: two types of trapezoidal cross-section, normal and reverse arched vault, normal and reverse triangular vault. We know that not all of these shapes occur commonly, but they are certainly important for understanding the anomalous wave field in their cases.

In Figure 4 we have an example of a cavity with relatively high vertical dimension (5 m), which does not occur very often in historical buildings (but there exist such examples). We chose this example because it clearly shows the manifestation of special multiple waves within the cavity itself. Reflection from the bottom edge (at TWT 53.3 ns) can be well seen in the results from ReflexW software (Fig. 4b), but it has a more complex shape in the results from the GPRmax algorithm (Fig. 4f). This is due to the fact that in the result from the GPRmax algorithm also the multiple from the top soil/air surface interferes with other reflections. Migration is very

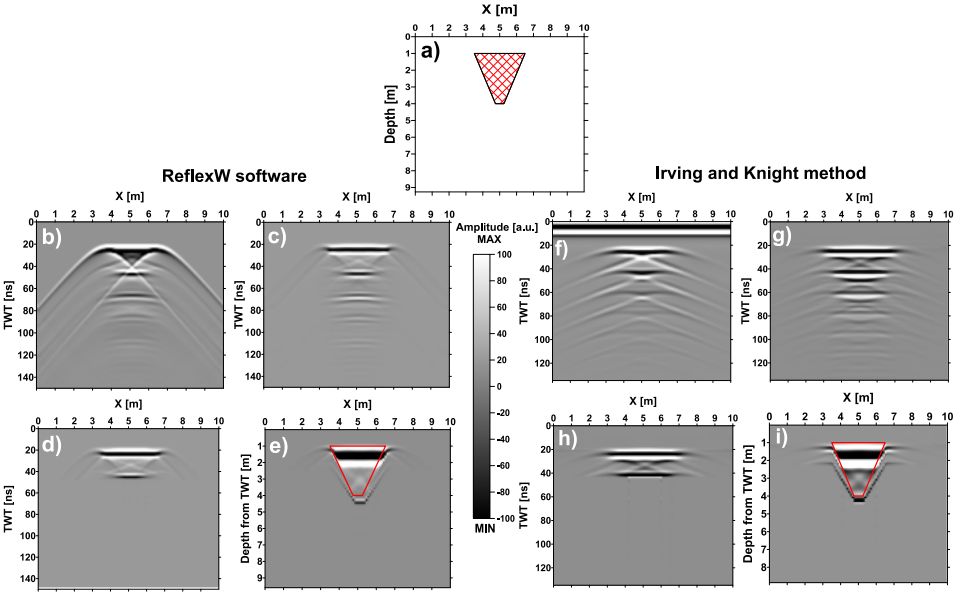

Fig. 6. Comparison of processed 2D synthetic radargrams of modelled cavity structure with trapezoidal cross-section (wider part at the top, height = 3 m). Explanation of panels a) – i) is identical with Figs. 4 and 5. In radargrams h) – i) additional removal of the multiple from the top of the model was not applied. Processing parameters used: summation width (applied during migration) = 75 for ReflexW results and 80 for the Irving and Knight method results, migration velocity = 0.1 m/ns.

helpful and makes the pattern much more clear (Fig. 4g), but the multiple from the top soil/air surface (TWT = 40 ns, as expected) is still present. By means of a simple in-house MATLAB script we have removed this multiple – by removing amplitudes that occur at integer multiples of the TWT value from the first important reflection (from the upper edge of the cavity). Result of this simple processing step (Fig. 4h) has very similar character, when compared with the result from the ReflexW method (Fig. 4d) (slightly different character of the amplitudes of the main reflecting boundaries in the results from the ReflexW software and GPRmax algorithm is given by the usage of different basic wavelets, involved in both methods). Finally, after application of the CTDC transformation (Fig. 4e and Fig. 4i), resulting depth-sections give a good representation of the horizontal/vertical extent of the cavity and its geometry (great difference of the wave pattern character can be seen mostly between images in Fig. 4f and Fig. 4i). The

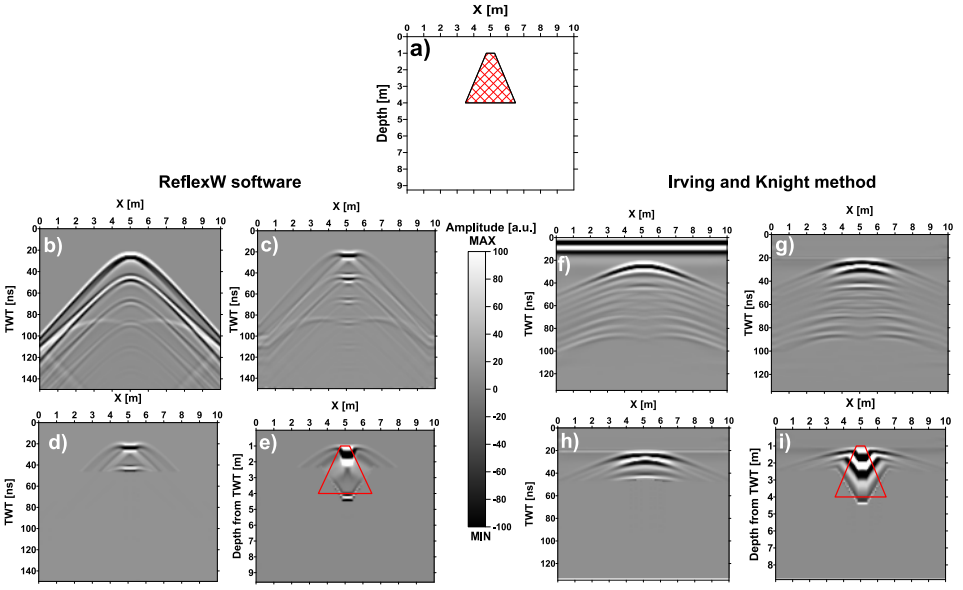

Fig. 7. Comparison of processed 2D synthetic radargrams of modelled cavity structure with trapezoidal cross-section (wider part at the bottom, height = 3 m). Explanation of panels a) – i) is identical with Figs. 4 and 5. In radargrams h) – i) additional removal of the multiple from the top of the model was not applied. Processing parameters used: summation width (applied during migration) = 75 for ReflexW results and 145 for the Irving and Knight method results, migration velocity = 0.1 m/ns.

only difference between Fig. 4 and Fig. 5 is that in the case of Fig. 5 the Irving-Knight method was used (parameters of the prism with rectangular cross-section are identical). As we can see, results from these two methods (GPRmax and Irving-Knight method) are very similar and helpful to understand better real-world GPR sections (B-scans).

In Figures 6 and 7 we present results from prisms with trapezoidal cross-section (Fig. 6: wider part in the top; Fig. 7: wider part in the bottom). Such types of cavities are not very common in the real world (mainly this in Fig. 6), but we wanted to show the wave pattern in 2D radargrams and the effects of the applied processing steps for these types of objects. In the received results, we can see how important is the role of the upper edge in the detection of the bottom one. In the case, when the upper edge has larger horizontal dimension than the bottom one – both of them are relatively well described in the migrated and corrected radargrams after applying the

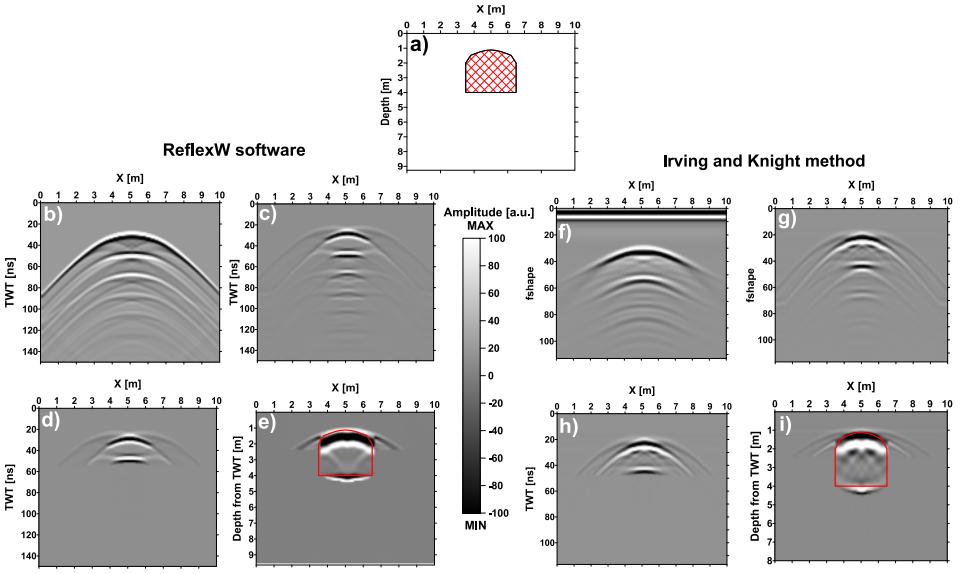

Fig. 8. Comparison of processed 2D synthetic radargrams of modelled cavity structure with a normal arched vault (bottom edge is flat, height = 3 m). Explanation of panels a) – i) is identical with Figs. 4 and 5. In radargrams h) – i) additional removal of the multiple from the top of the model was not applied. Processing parameters used: summation width (applied during migration) = 75 for ReflexW results and 145 for the Irving and Knight method results, migration velocity = 0.1 m/ns.

CTDC transformation (Fig. 6e and Fig. 6i). Trapezoidal shape of the cavity can be well recognised. Completely opposite situation is in the case of a cavity with small horizontal dimension – received geometry of the cavity in the final radargrams (Fig. 7e and Fig. 7i) is deformed and the trapezoidal shape cannot be interpreted in this case. Very similar results were received from cavities with triangular cross-sections (SM4-4 and SM4-5 in Supplementary Materials).

The model in Figure 8 is probably the closest to the real world examples – it is a cavity with normal arched vault. It can be seen, how the shape of the upper edge is influencing the shape of the bottom edge, even after applying the migration procedure (Fig. 8c and Fig. 8g) (this can be followed also in examples in Figs. SM3-1 and SM3-2 in the Supplementary material). The same influence is visible in the case of a cavity with a reverse arched vault (Fig. 9). Such a situation is really artificial (reverse vault), but again – it

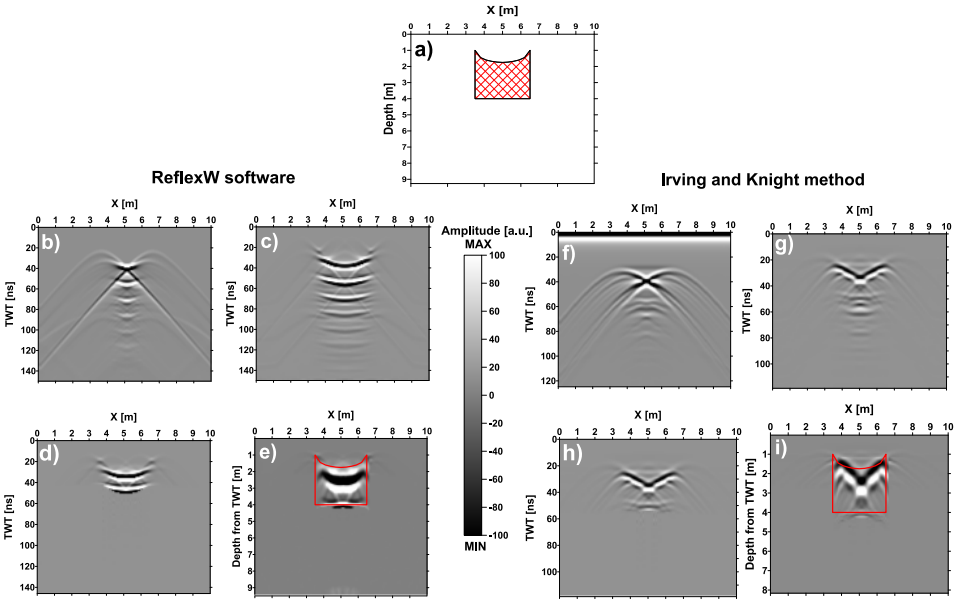

Fig. 9. Comparison of processed 2D synthetic radargrams of modelled cavity structure with a reverse arched vault (bottom edge is flat, height = 3 m). Explanation of panels a) – i) is identical with Figs. 4 and 5. In radargrams h) – i) additional removal of the multiple from the top of the model was not applied. Processing parameters used: summation width (applied during migration) = 75 for ReflexW results and 100 for the Irving and Knight method results, migration velocity = 0.1 m/ns.

shows nicely, how the shape of the bottom edge is influenced by the shape of the upper edge, even in migrated versions. In both cases, the CTDC transformation yields interesting results, where even the shape of bottom edge was slightly corrected (this was not the case for the Irving and Knight method, where the final result was influenced by an imperfect removal of the diffraction waves from the top corners of the cavity). In Figures 10 and 11 we have a similar situation, like it was in Figs. 8 and 9, but the shape of the upper boundary is triangular – with normal and reverse versions. In the situation with normal triangular shape (Fig. 10) the shape of the upper boundary could be well reconstructed in the final radargrams after all processing steps, but the shape of the bottom boundary could not be well estimated. In the case with reverse triangular shape (Fig. 11) the result is even worse – existence of the diffraction waves from the centre of the upper boundary makes the section more complicated and migration proce-

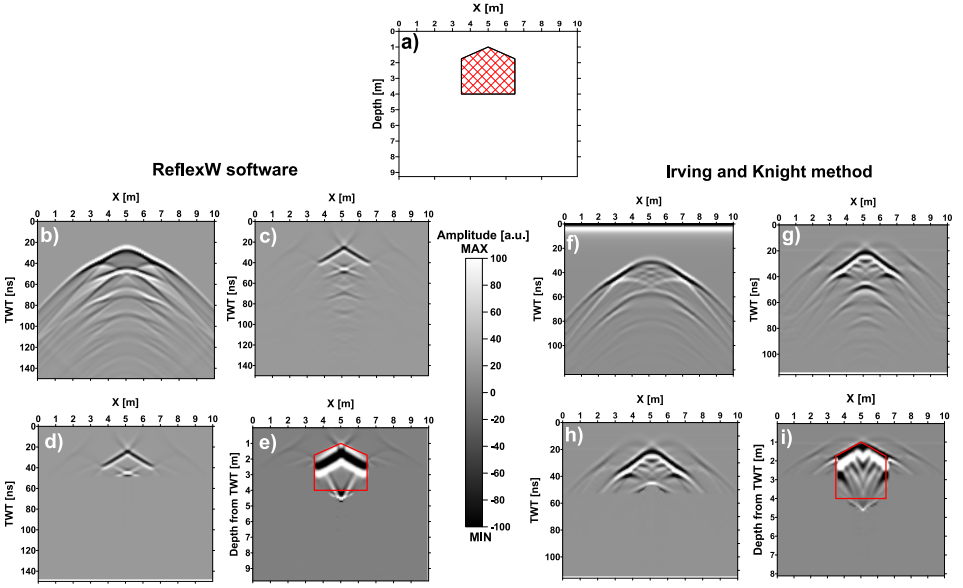

Fig. 10. Comparison of processed 2D synthetic radargrams of modelled cavity structure with a cross-section with normal triangular vault (bottom edge is flat, height = 3 m). Explanation of panels a) – i) is identical with Figs. 4 and 5. In radargrams h) – i) additional removal of the multiple from the top of the model was not applied. Processing parameters used: summation width (applied during migration) = 75 for ReflexW results and 145 for the Irving and Knight method results, migration velocity = 0.1 m/ns.

dure could not eliminate this influence completely. Imperfect estimation of the upper boundary shape has influenced also the estimation of the bottom boundary shape – so this result is one of the worst among all the calculated examples.

From examples SM2-1 to SM2-8 (cavity with rectangular cross-section, various horizontal dimensions) and SM3-1 to SM3-4 (cavity with normal arched vault, various horizontal dimensions) in Supplementary Materials we can observe several interesting properties of the received radargrams. The first important point is given by the fact that for larger horizontal dimensions the corners of the upper edge are always characterised by diffraction waves, which have the velocity of the upper soil layer (0.1 m/ns). Corners of bottom edges produce also diffraction waves, their velocity is close to the average velocity (0.2236 m/ns), calculated by the VRMS approach (Eq. 3), as it was shown in Fig. 1 and also in Figs. SM4-1 and SM4-2. The

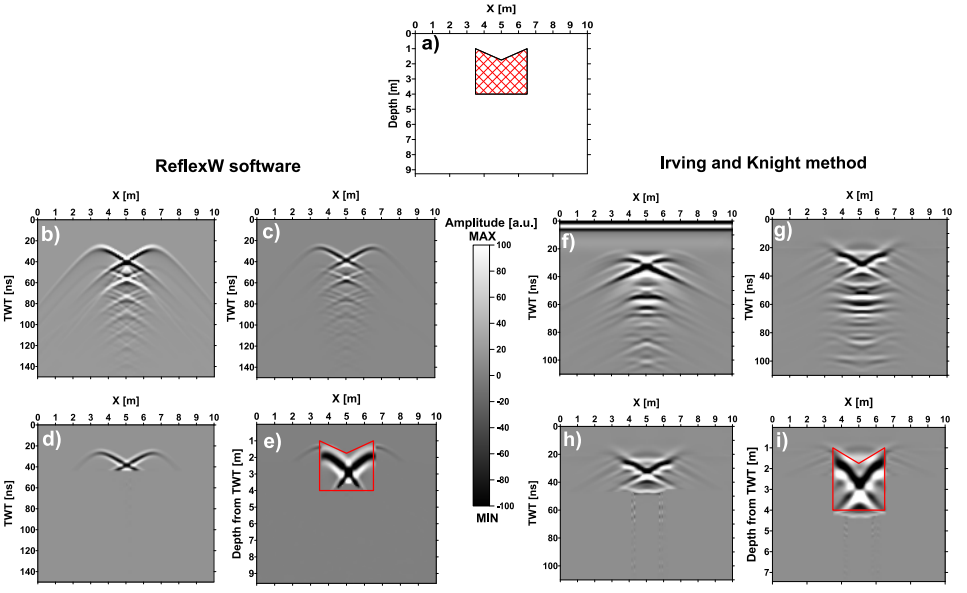

Fig. 11. Comparison of processed 2D synthetic radargrams of modelled cavity structure with a cross-section with reverse triangular vault (bottom edge is flat, height = 3 m). Explanation of panels a) – i) is identical with Figs. 4 and 5. In radargrams h) – i) additional removal of the multiple from the top of the model was not applied. Processing parameters used: summation width (applied during migration) = 75 for ReflexW results and 145 for the Irving and Knight method results, migration velocity = 0.1 m/ns.

second important point is that with very thin vertically stretched cavities (Figs. SM2-7 to SM2-8 and Figs. SM3-3 to SM3-4), we cannot reliably detect the diffracted wave from the bottom edge - only that from the upper edge. At this point, we cannot explain this phenomenon, but it is important to keep it in mind when interpreting real data.

In the case of a cavity with circular cross-section (Fig. SM4-3 in Supplementary Materials) we have received one dominant diffraction wave from the top edge of the object and from the bottom edge of the object (together with multiples of the first order). This result is in full agreement with the results presented in the text-book from *Reynolds (2011, p. 589, Fig. 14.29)*.

As an example of the application of the presented processing steps, we present the results of archaeo-geophysical measurements in the St. Catherine's church in Banská Štiavnica. Measurements in the interior of the church (GPR, microgravimetry, ERT = electrical resistivity tomography) were carried out as part of a joint exercise between the Christian-Albrechts University in Kiel and Comenius University in Bratislava (*Pašteka et al., 2019*). GPR measurements were performed on parallel lines with 0.3 m separation, in the central part of the church (close to the altar) by means of the GSSI equipment (400 MHz antenna, SIR-3000 controller). From the acquired data, we have selected a typical line, which was measured above an unknown cavity (verified also by microgravimetry and ERT survey), originally acquired data are displayed in Fig. 12a. In Fig. 12b we can see the processed result after applying dewow, zero-time removal, background removal, gain (energy decay) and Kirchhoff migration (summation width = 100 traces). Important features of the radargram are signed by yellow colour numbers: 1 – main reflection from the upper edge (vault, TWT = 9 ns) of the cavity, 2 – reflection from the bottom (with inversed polarity of amplitudes, TWT = 20 ns), 3 – multiple of second type from the top surface soil/air (TWT = 18 ns), 4 – this is probably the so-called dihedral (or corner) signal (*Martinaud et al., 2004*) or interference of several multiples of first and second order. When removing multiple waves, we focused mainly on the deeper parts of the processed radargram (TWT larger than 22 ns) (Fig. 12c), using the approach in ReflexW software. We did not remove the second type of multiple from the top surface soil/air (TWT = 18 ns), as it is located in close proximity to the reflection from the bottom of the cavity (such removal would have distorted or completely suppressed the bottom

cavity reflection). Final step was the CTDC transformation with a prepared velocity model (velocity for air was used in the expected space of the cavity – with upper vault and bottom flat floor). In the final depth-section we can see the resulting cavity geometry – in the depth interval from 0.5 m to

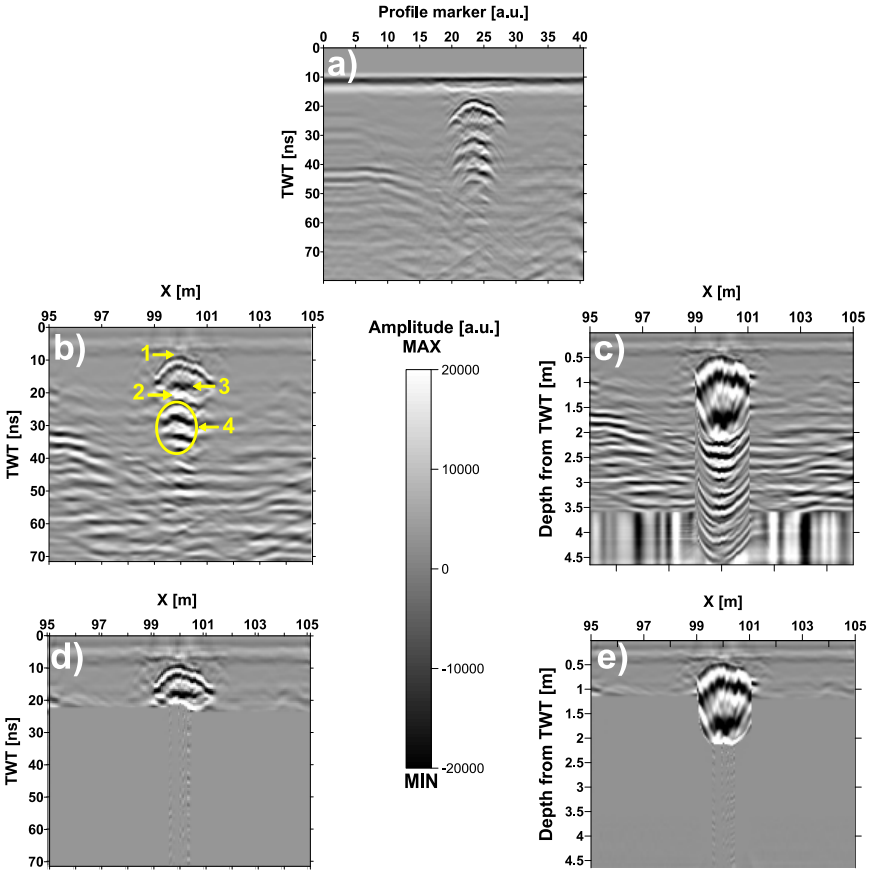

Fig. 12. Practical data example: selected GPR line (GSSI 400 MHz antenna) from the church of St. Catherine's in Banská Štiavnica. Panel a) shows the original acquired radargram (without any processing). Panel b) shows the result after applying dewow, zero-time removal, background removal, gain (energy decay) and migration (find the description of features 1–4 in the main text). Panel c) shows the radargram from b) with applied CTDC transformation. Panel d) shows the radargram from b) with multiples removal, performed with ReflexW. Panel e) shows the radargram in d) with applied CTDC transformation. Processing parameters used: dewow filter length = 4, summation width (applied during migration) = 100, migration velocity = 0.1 m/ns.

approx. 2.0 m). Of course, such a result is strongly influenced by the used velocity model and its geometry. The detected and interpreted cavity has not yet been verified by archaeological probing or video inspection, but it could probably be a crypt or a treasury chamber.

4. Conclusions

This paper presents several results from synthetic modelling of cavity responses in constant-offset 2D radargrams (by means of 3 independent FDTD methods) to better understand the results of real GPR measurements in such types of surveys. In addition to presenting anomalous wave fields in cavities with different cross-sectional shapes (main reflections from upper and bottom edges, intensive multiples and the presence of diffracted waves from the corners of the cavity edges), this study also focuses on the necessary processing steps that attempt to extract essential information about the cavities under investigation – their depth, dimensions, and shape. It can be stated that the depth and shape of the upper edge of the cavity can be determined unambiguously in the majority of situations, while all other parameters remain subject to interpretation. Migration is an extremely important step in the processing flow and it improves the detected shape of the upper cavity boundary. In our opinion, the final interpretation of cavity shapes should only be carried out on migrated sections. Very important is also the removal of multiples, which make the anomalous pattern in the radargram more complicated.

Another very important step is the application of the CTDC (Combined Time – Depth Conversion) transformation method (*Persico et al., 2024*), which recalculates the final time slices to their depth equivalents, including correct information about the speed of EM waves in air (inside the cavity). This method helps very much to improve the final radargrams (depth-sections) for interpretation. Vertical dimensions of cavities are in this result much more correct and in some cases also the geometry of the cavity is closer to its real shape. On the other hand, this kind of transformation can strongly influence the result, because the used velocity model pre-defines the final extension and shape of the resulting cavity geometry. This important processing step can be performed several times – with different velocity models and the final solution can be found by an iterative

way. CTDC method is limited in the case of cavities with irregular shapes – it works well, when the horizontal dimension of the upper cavity edge is larger than the horizontal dimension of its bottom edge.

Only cavities with very small horizontal dimensions are characterized by one dominant diffraction wave (e.g. *Liu et al., 2021*), in the case of cavities with larger horizontal dimensions the main reflection has the shape of the upper edge and corners of the edge are characterized by diffraction waves, which contribute to the creation of the typical "X-shaped feature" (*Utsi, 2017* in *Persico et al., 2019; Persico et al., 2024*). This feature can be in majority case easily removed by properly performed migration (the proper value of the summation width parameter must be found by trial-and-error method). These interesting patterns originate also in the case when the side walls of the cavity are not vertical (e.g. Fig. 6 and SM4-2 in Supplementary Material).

Shapes and horizontal dimensions of the reflections from detected bottom edge have their typical properties (e.g. inverse polarity of reflection amplitudes) and are strongly influenced by the shape and horizontal extension of the upper edge. Removal of some of the multiples can influence the detection of the bottom edge reflection and must be performed in a sensitive manner, when dealing with real-world datasets.

Demonstrated properties of 2D radargrams in the case of synthetically modelled cavities are compared with real-world data-sets, one of them we have presented also here – results of archaeo-geophysical measurements in the St. Catherine's church in Banská Štiavnica. This case study confirms our experiences from synthetic studies and the applicability of suggested processing steps (among them mainly migration and the so-called Combined Time – Depth Conversion transformation). The research results provide direct applications for archaeological prospection and civil engineering projects because they enable precise identification of underground voids which protects sites from damage and ensures public safety. In the future we would like to expand our studies also to 3D cases of synthetic modelling and joint interpretation with other geophysical methods (e.g. microgravimetry).

Acknowledgements. The presented results have been performed with the support from scientific project VEGA 1/0587/24. The authors would like to express their thanks to all students and colleagues from the Christian-Albrechts University in Kiel and

from the Comenius University in Bratislava, who helped with the data acquisition in the St. Catherine's church in Banská Štiavnica. The authors are also grateful for valuable comments and suggestions for corrections from the invited reviewers. Parts of the text of this paper were translated with DeepL.com (free version).

References

Annan A. P., 2003: Ground Penetrating Radar: Principles, Procedures and Applications. Sensors & Software Inc., Mississauga, Canada, 286 p.

Basile V., Carrozzo M. T., Negri S., Nuzzo L., Quarta T., Villani A. V., 2000: A ground-penetrating radar survey for archaeological investigations in an urban area (Lecce, Italy). J. Appl. Geophys., **44**, 1, 15–32, doi: 10.1016/S0926-9851(99)00070-1.

Bergmann T., Robertsson J. O. A., Holliger K., 1996: Numerical properties of staggered finite-difference solutions of Maxwell's equations for ground-penetrating radar modelling. Geophys. Res. Lett., **23**, 1, 45–48, doi: 10.1029/95GL03515.

Bourgeois J. M., Smith G. S., 1996: A Fully Three-Dimensional Simulation of a Ground-Penetrating Radar: FDTD Theory Compared with Experiment. IEEE Trans. Geosci. Remote Sens., **34**, 1, 36–44, doi: 10.1109/36.481890.

Cai J., McMechan G. A., 1995: Ray-based synthesis of bistatic ground-penetrating radar profiles. Geophysics, **60**, 1, 87–96, doi: 10.1190/1.1443766.

Carcione J. M., 1996: Ground-penetrating radar: Wave theory and numerical simulation in lossy anisotropic media. Geophysics, **61**, 6, 1664–1677, doi: 10.1190/1.1444085.

Casper D. A., Kung K.-J. S., 1996: Simulation of ground-penetrating radar waves in a 2-D soil model. Geophysics, **61**, 4, 1034–1049, doi: 10.1190/1.1444025.

Cuenca-Garcia C., Asăndulesei A., Lowe K. M. (Eds.}, 2024: World Archaeo-Geophysics: Integrated minimally invasive approaches using country-based examples. Springer, 482 p., doi: 10.1007/978-3-031-57900-4.

Daniels D. J., 2004: Ground Penetrating Radar (2nd Edition). The Institution of Electrical Engineers, London, 752 p., doi: 10.1049/pbra015e.

Giannopoulos A., 2005: Modelling ground penetrating radar by GprMax. Constr. Build. Mater., **19**, 10, 755–762, doi: 10.1016/j.conbuildmat.2005.06.007.

Goodman D., 1994: Ground-penetrating radar simulation in engineering and archaeology. Geophysics, **59**, 2, 224–232, doi: 10.1190/1.1443584.

GPRmax website, n.d.: GPRmax: Finite-Difference Time-Domain Electromagnetic simulation software. https://www.gprmax.com/about.shtml, accessed on 18 September 2025.

Haynes I., Ravasi T., Kay S., Piro S., Liverani P. (Eds.), 2023: Non-Intrusive Methodologies for Large Area Urban Research. Archaeopress, 130 p.

Irving J., Knight R., 2006: Numerical modeling of ground-penetrating radar in 2-D using MATLAB. Comput. Geosci., **32**, 9, 1247–1258, doi: 10.1016/j.cageo.2005.11.006.

Kuhns G. L., 1983: Application of Ground Penetrating Radar to the Detection of Subsurface Cavities. PhD. thesis, University of Central Florida, 78 p.

Leckebusch J., 2000: Two- and Three-dimensional Ground penetrating Radar Surveys Across a Medieval Choir: a Case Study in Archaeology. Archaeol. Prospect., **7**, 3, 189–200, doi: 10.1002/1099-0763(200009)7:3<189::AID-ARP134>3.0.CO;2-N.

Leucci G., De Giorgi L., 2010: Microgravimetric and ground penetrating radar geophysical methods to map the shallow karstic cavities network in a coastal area (Marina Di Capilungo, Lecce, Italy). Explor. Geophys., **41**, 2, 178–188, doi: 10.1071/EG09029.

Leucci G., De Giorgi L., Ditaranto I., Miccoli I., Scardozzi G., 2021: Ground-Penetrating Radar Prospections in Lecce Cathedral: New Data about the Crypt and the Structures under the Church. Remote Sens., **13**, 9, 1692, doi: 10.3390/rs13091692.

Linford N., 2006: The application of geophysical methods to archaeological prospection. Rep. Prog. Phys., **69**, 7, 2205–2257, doi: 10.1088/0034-4885/69/7/R04.

Liu Q. H., Fan G.-X., 1999: Simulations of GPR in dispersive media using a frequency-dependent PSTD algorithm. IEEE Trans. Geosci. Remote Sens., **37**, 5, 2317–2324, doi: 10.1109/36.789628.

Liu H., Shi Z., Li J., Liu C., Meng X., Du Y., Chen J., 2021: Detection of road cavities in urban cities by 3D ground-penetrating radar. Geophysics, **86**, 3, WA25–WA33, doi: 10.1190/GEO2020-0384.1.

Lorenzo H., Hernandez M. C., Cuéllar V., 2002: Selected radar images of man-made underground galleries. Archaeol. Prospect., **9**, 1, 1–7, doi: 10.1002/arp.174.

Martinaud M., Frappa M., Chapoulie R., 2004: GPR signals for the understanding of the shape and filling of man-made underground masonry. Proceedings of the 10th International Conference on Ground Penetrating Radar, 21-24 June, Delft, The Netherlands, ARC.2, 439–442, doi: 10.1109/ICGPR.2004.179770.

Morey R. M., 1974: Detection of subsurface cavities by ground penetrating radar. US Highway Geological Symposium Proc., **27**, 28–30.

Panisova J., Murín I., Pašteka R., Haličková J., Brunčák P., Pohánka V., Papčo J., Milo P., 2016: Geophysical fingerprints of shallow cultural structures from microgravity and GPR measurements in the Church of St. George, Svätý Jur, Slovakia. J. Appl. Geophys., **127**, 102–111, doi: 10.1016/j.jappgeo.2016.02.009.

Pašteka R., Kušnirák D., Wilken D., Putiška R., Papčo J., Godová D., Zvara I., Nogová E., Ondrášová L., 2019: Effective combination of microgravimetry and geoelectrical methods in the detection of subsurface cavities in archaeological prospection – selected case-studies from Slovakia. Contrib. Geophys. Geod., **49**, 4, 479–496, doi: 10.2478/congeo-2019-0025.

Persico R., Ciminale M., Matera L., 2014: A new reconfigurable stepped frequency GPR system, possibilities and issues; applications to two different Cultural Heritage Resources. Near Surf. Geophys., **12**, 6, 793–801, doi: 10.3997/1873-0604.2014035.

Persico R., D'Amico S., Matera L., Colica E., De Giorgio C., Alescio A., Sammut C., Galea P., 2019: GPR Investigations at St John's Co-Cathedral in Valletta. Near Surf. Geophys., **17**, 3, 213–229, doi: 10.1002/nsg.12046.

Persico R., Catapano I., Esposito G.; Morelli G., De Martino G., Capozzoli L., 2024: GPR Mapping of Cavities in Complex Scenarios with a Combined Time–Depth Conversion. Sensors, **24**, 10, 3238, doi: 10.3390/s24103238.

Pozar D. M., 2012: Microwave Engineering (4th ed.). John Wiley & Sons Inc., 732 p.

Prokopidis K. P., Tsiboukis T. D., 2007: Modeling of Ground-Penetrating Radar for Detecting Buried Objects in Dispersive Soils. Appl. Comput. Electromagn. Soc. J., **22**, 2, 287–294.

Reynolds J. M., 2011: An Introduction to Applied and Environmental Geophysics. Wiley-Blackwell, 696 p.

Sandmeier K. J., 2020: REFLEXW Version 9.5 manual. Manuscript, 709 p., accessible at https://www.sandmeier-geo.de/.

Smith D. G., Jol H. M., 1995: Ground penetrating radar: antenna frequencies and maximum probable depths of penetration in Quaternary sediments. J. Appl. Geophys., **33**, 1-3, 93–100, doi: 10.1016/0926-9851(95)90032-2.

Solla M., Lorenzo H., Pérez-Gracia V., 2016: Ground penetrating radar: Fundamentals, methodologies and applications in structures and infrastructure. In: Riveiro B., Solla M. (Eds.): Non-Destructive Techniques for the Reverse Engineering of Structures and Infrastructure. Taylor & Francis Group, 89–111.

Teixeira F. L., Chew W. C., Straka M., Oristaglio M. L., Wang T., 1998: Finite-Difference Time-Domain Simulation of Ground Penetrating Radar on Dispersive, Inhomogeneous, and Conductive Soils. IEEE Trans. Geosci. Remote Sens., **36**, 6, 1928–1937, doi: 10.1109/36.729364.

Utsi E. C., 2017: Ground Penetrating Radar: Theory and Practice. Butterworth-Heinemann, Amsterdam, 205 p.

Wang T., Tripp A. C., 1996: FDTD simulation of EM wave propagation in 3-D media. Geophysics, **61**, 1, 110–120, doi: 10.1190/1.1443930.

Warren C., Giannopoulos A., Giannakis I., 2016: gprMax: Open source software to simulate electromagnetic wave propagation for Ground Penetrating Radar. Comput. Phys. Commun., **209**, 163–170, doi: 10.1016/j.cpc.2016.08.020.

Yilmaz Ö., 2001: Seismic Data Analysis: Processing, Inversion, and Interpretation of Seismic Data. Society of Exploration Geophysicists, Tulsa, doi: 10.1190/1.9781560801580.

Zeng X., McMechan G. A., Cai J., Chen H.-W., 1995: Comparison of ray and Fourier methods for modeling monostatic ground penetrating radar profiles. Geophysics, **60**, 6, 1727–1734, doi: 10.1190/1.1443905.